ISSN 0036-0236, Russian Journal of Inorganic Chemistry, 2021, Vol. 66, No. 4, pp. 490–495. © The Author(s), 2021. This article is an open access publication, corrected publication 2021.
Russian Text © The Author(s), 2021, published in Zhurnal Neorganicheskoi Khimii, 2021, Vol. 66, No. 4, pp. 464–469.

SYNTHESIS AND PROPERTIES OF INORGANIC COMPOUNDS

Synthesis of $CaCu_3Ti_4O_{12}$: How Heat Treatment Influences Morphology and Dielectric Properties

K. V. Ivanov[a], *, A. V. Noskov[a], O. V. Alekseeva[a], and A. V. Agafonov[a]

[a] *G.A. Krestov Institute of Solution Chemistry, Russian Academy of Sciences, Ivanovo, 153045 Russia*

**e-mail: ivk@isc-ras.ru*

Received October 14, 2020; revised October 14, 2020; accepted October 19, 2020

Abstract—A ceramic powder, the precursor of $CaCu_3Ti_4O_{12}$, was prepared by liquid-phase synthesis in acetic acid. The synthesized samples were calcined at 200, 400, 600, 800, and 1100°C and then characterized by a set of physicochemical methods. An increase in annealing temperature induced changes in the particle size distribution and quantitative porosity parameters of the powder. Analysis of the dielectric spectra of suspensions of synthesized materials allowed us to conclude that high-temperature annealing of the powder leads to a decrease in relaxation time.

Keywords: $CaCu_3Ti_4O_{12}$, synthesis, dielectric spectra, morphology, heat treatment

DOI: 10.1134/S0036023621040136

INTRODUCTION

In recent years, the attention of researchers has been directed to ceramic materials with the perovskite structure due to their potential for use in high-frequency electronics, for the production of capacitors, generators, and filters [1]. Barium, strontium, and calcium titanates are just such materials, but these perovskites exhibit an abrupt change in dielectric constant near the Curie temperature, and this largely limits their practical applicability.

Among the perovskite-like oxides, one can distinguish calcium copper titanate $CaCu_3Ti_4O_{12}$ (CCTO) and related materials. The dielectric constant of this compound changes little over a wide temperature range up to 600 K; so, CCTO is suitable for use in design of microelectronic elements, namely, capacitors, microwave devices, gas sensors, automotive electronic devices, random access memory devices, etc. [2, 3].

The development of new synthesis methods for preparing nanoscale $CaCu_3Ti_4O_{12}$ is of great interest with the view of reducing the size of electronic elements, increasing their efficiency and productivity. Solid-phase synthesis is the most common method for preparing CCTO, like for most perovskites, due to its facility [4–8]. Along with calcium copper titanate, however, this synthesis can also yield copper(II) oxide, which fills-in intergrain spaces of the ceramics and influences the functional properties of the material. In addition, the heat treatment of the initial components of the mixture takes more than 1 h, and leads to significant energy costs in the production of CCTO [9].

Other methods for preparing $CaCu_3Ti_4O_{12}$ are also described in the literature, among them, liquid-phase synthesis (including a sol–gel process), combustion synthesis, coprecipitation, and other processes [10–16]. The advantage of liquid-phase synthetic methods over solid-phase methods is a lower process temperature and the ability to provide the exact stoichiometry and uniform phase composition of the powders. Depending on the used liquid-phase synthesis technique, it is possible to control not only the particle size, but also the shape, specific surface, area and pore structure of the particles. Zhao et al. [17] employed the sol–gel process followed by annealing at 900°C for 2 h to produce CCTO powders with particle sizes less than 100 nm.

Ahmadipour et al. [10] in their survey provide data on the influence of the $CaCu_3Ti_4O_{12}$ preparation conditions (annealing temperature and process time) and impurities on the product dielectric properties; they also show the relevance of such studies for solving both fundamental and applied problems.

This work is a continuation of the earlier study [18] where the thermal evolution of the CCTO ceramic powder precursor and its photocatalytic activity were studied by X-ray phase analysis, mass spectroscopy, thermal analysis, UV and IR spectroscopy. The study showed that $CaCu_3Ti_4O_{12}$ phase formation is over by 1100°C.

In the article presented here, the CCTO precursor was synthesized by the liquid-phase method and stud-

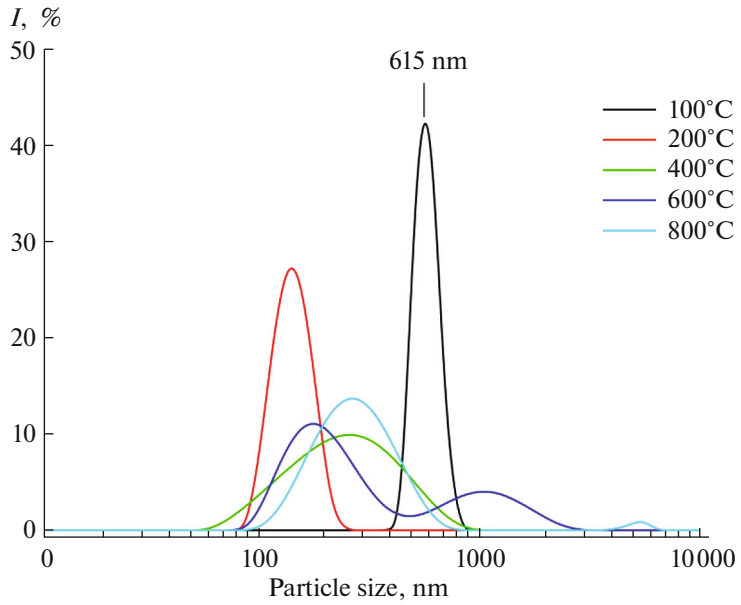

Fig. 1. Particle-size distribution diagrams for powders annealed at various temperatures.

ies of its physicochemical properties depending on the heat treatment temperature were continued. In particular, dynamic light scattering, nitrogen vapor sorption–desorption, and dielectric spectroscopy were used.

EXPERIMENTAL

The precursor of CCTO ceramic powder was prepared by a liquid-phase method in acetic acid. The initial reagents used were $Ca(OH)_2$, $Cu(CH_3COO)_2{\cdot}H_2O$, and $Ti(C_4H_9O)_4$ (Sigma-Aldrich) taken in the CaO : CuO : TiO_2 = 1 : 3 : 4 stoichiometry. The first synthesis step involved the preparation of a $Cu(CH_3COO)_2{\cdot}H_2O$ solution in water and a $Ca(OH)_2$ solution in acetic acid. Then, the solutions were mixed together and then stirred for 1 h at 85°C. To the resulting homogeneous mixture, $Ti(C_4H_9O)_4$ was added dropwise and was also kept for 1 h at 85°C under continuous stirring. Then, the solution was concentrated to a constant weight in a drying cabinet at 100°C, and the thus-obtained sample was annealed in air at 200, 400, 600, 800, and 1100°C.

Heat-treated powder samples were studied by a set of physicochemical methods.

Particle size compositions in the range from 0.3 nm to 10 μm were determined on a Zetasizer Nano ZS (Malvern Instruments) laser diffraction analyzer. The powders were pretreated in an ultrasonic bath in isopropyl alcohol for 1 h in order to destroy agglomerates.

The specific surface areas and quantitative characteristics of the porous structure of annealed samples of the synthesized powder were estimated based on the analysis of low-temperature (77 K) nitrogen vapor adsorption–desorption isotherms. Isotherms were recorded using a QuantaChrome Nova 1200 high-speed gas sorption analyzer.

Dielectric properties were measured in 30% suspensions of prepared materials using an E7-20 RCL meter at frequencies in the range from 25 to 10^6 Hz in a capacitor cell. The required amounts of the solid phase and PMS-20 (PENTA) silicone oil were thoroughly triturated in an agate mortar for 2 h until a homogeneous stable suspension was obtained. What silicone oil is used in the work means the need to study its effect on the behavior of the CCTO precursor powder, while it is heat-treated to be converted to $CaCu_3Ti_4O_{12}$, on the dielectric characteristics in the liquid phase. In choosing silicon oil (PMS-20) we were guided by its high performance characteristics: a wide operating temperature range (–60 to +200°C) and a high breakdown voltage (>7 kV/mm).

RESULTS AND DISCUSSION

Particle Size Distribution

Figure 1 shows particle-size distribution diagrams for the tested powder depending on the annealing temperature. Clearly, the transverse sizes are in the range from 100 to 2000 nm for almost all particles. For the powder annealed at 100°C, the distribution curve is monomodal with a peak at 615 nm. The increasing annealing temperature leads to an increase in the proportion of smaller particles. In addition, the distributions for 600 and 800°C are bimodal.

Pore Structure

The porosity studies on annealed samples of $CaCu_3Ti_4O_{12}$ precursors involving low-temperature nitrogen adsorption–desorption measurements showed that, regardless of the annealing temperature, the resulting isotherms were type IV in terms of the IUPAC classification [19]. Wide hysteresis (Fig. 2) indicates micro- and mesopores in the material.

The Brunauer–Emmett–Teller (BET), Barrett–Joyner–Halenda (BJH), and Frankel–Halsey–Hill (FHH) models [20–25] were used to fit the experimental data for quantifying the porosity of the studied powders. In the calculations it was set that the cross-sectional area of the N_2 molecule is 0.162 nm^2, the N_2 monolayer thickness is 0.354 nm, and the density of liquid nitrogen is 0.808 g/cm^3.

The values of texture parameters derived from the isotherms for $CaCu_3Ti_4O_{12}$ precursor samples annealed at 200, 400, 600, 800, and 1100°C, appear in Table 1. These are the following parameters:

S_{BET} and S_{BJH} are the total surface area calculated using the BET and BJH models, respectively;

V_T is the total pore volume determined as the liquid nitrogen volume corresponding to the amount of nitrogen adsorbed at the relative pressure $p/p_0 = 0.99$; D_{avg} is the average pore diameter; and D_{prob} is the most probable pore diameter corresponding to the particle-size distribution peak.

From Table 1, one may infer that for samples annealed at 400°C, the pore volume is more than 10 times the respective value for samples annealed at 200°C. This result is consistent with the thermal analysis and mass spectrometry data presented earlier [19]; from those data, it flows that water, acetate groups, and acetone are removed when the as-synthesized powder is heated to 320°C. Therefore, we may assume that a significant volume of pore space is freed up due to this removal, to become accessible to nitrogen.

The specific surface areas of annealed samples were determined using the BET and BJH models. S_{BET} and S_{BJH} decrease when the annealing temperature becomes higher than 400°C (Table 1). One can also see some difference between the values determined in terms of the two models. This difference is likely to arise from the different postulates of these models. The BJH model, for example, is based on Kelvin's theory of filling-in cylindrical pores, while the BET theory has no this assumption.

Figure 3 shows pore-size distribution diagrams. The diagrams represent the proportions (in percent of the total pore space V_1 and V_2) corresponding to small (<11 nm in diameter) and large (>11 nm) pores. For almost all of the annealed samples (except for those annealed at 800°C), most nitrogen is adsorbed in pores with diameters less than 11 nm. The average pore sizes are in the range from 5.3 to 8.7 nm.

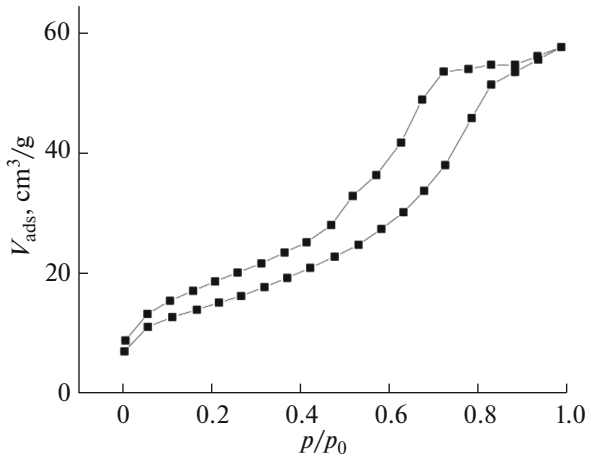

Fig. 2. Nitrogen sorption–desorption isotherm for the $CaCu_3Ti_4O_{12}$ precursor annealed at 600°C.

The data presented in Fig. 3 indicate that nonlinear changes in pore size are observed during the heat treatment of the CCTO precursor. For <11 nm pore diameters, these changes are due to certain physicochemical processes, namely, removal of physisorbed and chemisorbed water at 100–250°C and removal of excessive acetic acid and thermal destruction products of organic inclusions of the initial components upon heating to 600°C. The decreased percentage of these pores (V_1) at 800°C is likely to arise from sintering. The subsequent increase in the pore space of these pores at 1100°C is most likely due to phase modifications in the material that bring CCTO formation to the end.

For large pores (>11 nm in diameter), an inhomogeneous change is also observed with increasing temperature. Before 600°C the pore space decreases due to sintering. At 800°C, however, an opposite effect is observed, apparently associated with the removal at this temperature of carbonate groups produced in the reaction of the sample with CO_2 from the environment. Accordingly, further annealing at 1100°C again leads to sintering with a subsequent decrease in the percentage of large pores (V_2).

Table 1. Porosity parameters of annealed $CaCu_3Ti_4O_{12}$ precursor samples

Parameter	Annealing temperature, °C				
	200	400	600	800	1100
S_{BET}, m^2/g	4.283	83.669	54.074	35.234	2.078
S_{BJH}, m^2/g	3.628	70.903	61.914	20.746	2.266
V_T, cm^3/g	0.008	0.110	0.090	0.077	0.003
D_{avg}, nm	7.162	5.305	6.633	8.697	6.174
D_{prob}, nm	3.984	3.571	4.016	3.144	4.012

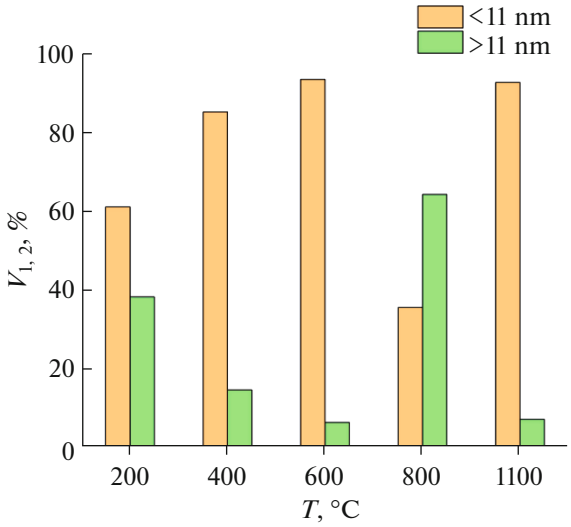

Fig. 3. Pore-size distribution versus pore size for as-synthesized powders annealed at various temperatures.

The inhomogeneity of the materials was quantified in terms of the FHH fractal model [24, 25]; namely, low-temperature N_2 vapor adsorption–desorption was used to determine d_f, the fractal dimension of the surface of a porous material.

According to Pomonis and Tsaous [24], the FHH method can calculate the fractal dimension of the adsorbent surface taking into account the effects of adsorbate surface tension, where the liquid/gas surface tension (capillary force) tends to decrease the interface area. The analytical expression for the FHH isotherm in this case is

$$\frac{V_{ads}}{V_m} \approx \left[RT \log\left(\frac{p_o}{p}\right)\right]^{d_f-3}, \qquad (1)$$

where R is universal gas constant, T is absolute temperature, V_{ads} is adsorbed gas volume, and V_m is volume required for one monolayer to form. From relationship (1) it flows that d_f can be calculated from the slope of the $\log(V_{ads})$ versus $\log\left(\log\left(\frac{p_o}{p}\right)\right)$ plot. The fractal dimensions found in this way for the adsorption and desorption branches of the isotherms appear in Table 2.

Table 2. Surface fractal dimensions of the CCTO precursor depending at various annealing temperatures in terms of the FHH model

Annealing temperature, °C	d_f	
	adsorption	desorption
200	2.637	2.713
400	2.661	2.695
600	2.645	2.659
800	2.623	2.627

The fractal dimension decreases as the annealing temperature increases starting with 400°C. This trend indicates a reduction in surface profile and is consistent with the trends toward reductions in specific area and pore space elucidated by BET and BJH.

Dielectric Measurements

We studied how heat treatment influenced the frequency-dependent dielectric constant and dielectric loss tangent in suspensions of prepared powders in silicon oil. The results appear in Fig. 4. One can see that dielectric constant dispersion is observed in the range 25–10^6 Hz. The tanδ values do not exceed 0.1 for the untreated powder (Fig. 4a). For a high annealing temperature (1100°C), the tanδ does not exceed 0.03 at frequencies in the range from 100 to 10^6 Hz (Fig. 4b).

In terms of the Debye theory, the analytical relation for the dielectric constant as a function of AC cyclic frequency ($\omega = 2\pi f$) is

$$\varepsilon = \varepsilon_\infty + \frac{\varepsilon_{st} - \varepsilon_\infty}{1 + (\omega\tau)^2}, \qquad (2)$$

where ε_{st} is static dielectric constant (when $\omega \to 0$); ε_∞ is high-frequency dielectric constant (when $\omega \to \infty$); and τ is relaxation time, i.e., the time required for the transition of the system from a nonequilibrium state to an equilibrium state.

Here, we used Eq. (2) for processing experimental frequency-dependent dielectric constant data, in order to calculate the relaxation times for the studied suspensions of synthesized powders. Annealing was found to decrease the relaxation time in powders: τ is 3.1×10^{-4} s for an untreated powder, while for a sample annealed at 1100°C, $\tau = 3.5 \times 10^{-5}$ s.

CONCLUSIONS

Our study shows that the precursor of CCTO ceramic powders prepared by liquid-phase synthesis experiences significant changes upon heat treatment. In particular, the particle size composition of the powder, pore structure characteristics, and dielectric relaxation parameters change. The observed thermal evolution is likely to arise from the formation of a $CaCu_3Ti_4O_{12}$ phase, which is over by 1100°C as probed by X-ray powder diffraction.

ACKNOWLEDGMENTS

The authors express their gratitude to the Upper Volga Regional Center for Physical and Chemical Research, a center for collective use of scientific equipment.

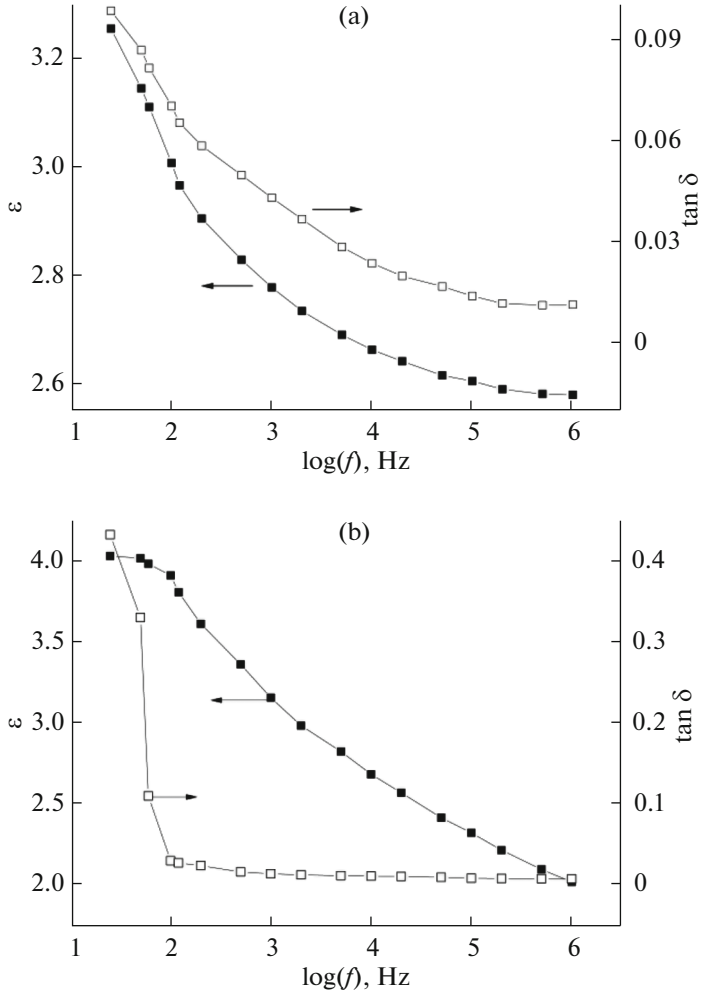

Fig. 4. Frequency-dependent dielectric constant and dielectric loos tangent for suspensions of as-synthesized powders: (a) without heat treatment and (b) after being annealed at 1100°C.

FUNDING

This work was supported by the Russian Science Foundation for Basic Research (project no. 18-43-370015-r-tsentr-a).

CONFLICT OF INTEREST

The authors declare that they have no conflict of interest.

OPEN ACCESS

REFERENCES

1. A. K. Raia, K. D. Mandala, D. Kumar, et al., J. Mater. Chem. Phys. **122**, 217 (2010). https://doi.org/10.1016/j.matchemphys.2010.02.037
2. P. Liu, Y. Lai, Y. Zeng, et al., J. Alloys Compd. **650**, 59 (2015). https://doi.org/10.1016/j.jallcom.2015.07.247
3. C. C. Homes, T. Vogt, S. M. Shapiro, et al., **293**, 673 (2001). https://doi.org/10.1126/science.1061655
4. B. Wang, Y. P. Pu, H. D. Wua, et al., Ceram. Int. **39**, 525 (2013). https://doi.org/10.1016/j.ceramint.2012.10.127

5. Z. Tang, Y. Huang, K. Wu, et al., J. Eur. Ceram. Soc. **38**, 1569 (2018). https://doi.org/10.1016/j.jeurceramsoc.2017.11.018
6. R. Schmidt, M. C. Stennett, N. C. Hyatt, et al., J. Eur. Ceram. Soc. **32**, 3313 (2012). https://doi.org/10.1016/j.jeurceramsoc.2012.03.040
7. S. D. Almeida-Didry, S. Merad, C. Autret-Lambert, et al., Solid State Sci. **109** (2020). https://doi.org/10.1016/j.solidstatesciences.2020.106431
8. S. D. Almeida-Didry, C. Autret, C. Honstettre, et al., Solid State Sci. **61**, 102 (2016). https://doi.org/10.1016/j.solidstatesciences.2016.07.010
9. N. A. Sekushin, N. A. Zhuk, L. A. Koksharova, et al., Lett. Mater. **9**, 5. https://doi.org/10.22226/2410-3535-2019-1-5-10
10. M. Ahmadipour, M. F. Ain, and Z. A. Ahmad, J. Nano-Micro Lett. **8**, 291 (2016). https://doi.org/10.1007/s40820-016-0089-1
11. W. X. Yuan, S. K. Hark, W. N. Mei, et al., J. Electrochem. Soc. **157**, 117 (2010). https://doi.org/10.1149/1.3353040
12. W. M. Hua, Z. Fu, W. Q. Li, et al., J. Cent. South Univ. **19**, 3385 (2012). https://doi.org/10.1007/s11771-012-1418-2
13. N. Banerjee and S. B. Krupanidhi, Curr. Nanosci. **6**, 432 (2010). https://doi.org/10.2174/157341310791658955
14. K. M. Kim, S. J. Kim, J. H. Lee, et al., J. Eur. Ceram. Soc. **27**, 3991 (2007). https://doi.org/10.1016/j.jeurceramsoc.2007.02.081
15. A. V. Agafonov, K. V. Ivanov, O. I. Davydova, et al., Russ. J. Inorg. Chem. **56**, 1025 (2011). https://doi.org/10.1134/S0036023611070035
16. J. Zhao, J. Liu, and G. Ma, Ceram. Int. **38**, 1221 (2012). https://doi.org/10.1016/j.ceramint.2011.08.052
17. J. Zhao, J. Liu, and G. Ma, J. Ceram. Int. **38**, 1221 (2012). https://doi.org/10.1016/j.ceramint.2011.08.052
18. K. V. Ivanov, O. V. Alekseeva, and A. V. Agafonov, Russ. J. Inorg. Chem. **65**, 1338 (2020). https://doi.org/10.1134/S0036023620100095
19. K. S. W. Sing, D. H. Everett, R. A. W. Haul, et al., Pure Appl. Chem. **57**, 603 (1985). https://doi.org/10.1515/iupac.57.0007
20. E. P. Barrett, L. G. Joyner, and P. P. Halenda, J. Am. Chem. Soc. **73**, 373 (1951). https://doi.org/10.1021/ja01145a126
21. K. S. W. Sing, Adv. Coll. Interf. Sci. **76–77**, 3 (1998). https://doi.org/10.1016/s0001-8686(98)00038-4
22. K. K. Aligizaki, *Pore Structure of Cement-Based Materials: Testing Interpretation and Requirements (Modern Concrete Technology)* (Taylor & Francis, New York, 2005). https://doi.org/10.1201/9781482271959
23. V. Panella and J. Krim, Stud. Surf. Sci. Catal. **87**, 91 (1994). https://doi.org/10.1016/s0167-2991(08)63068-2
24. P. J. Pomonis and E. T. Tsaous, Langmuir **25**, 9986 (2009). https://doi.org/10.1021/la901121c
25. L.-E. Sandoval-Diaz, J.-A. Aragon-Quiroz, Y.-S. Ruiz-Cardona, et al., Micropor. Mesopor. Mater. **237**, 260 (2017). https://doi.org/10.1016/j.micromeso.2016.08.030

Translated by O. Fedorova